



## Regulation of phonon localization on thermal transport in complex networks

Kezhao Xiong <sup>1,2,\*</sup> Yuqi Liu,<sup>1</sup> Man Zhou <sup>1</sup> Hang Dong,<sup>1</sup> and Zhengxin Yan<sup>1</sup>

<sup>1</sup>College of Sciences, Xi'an University of Science and Technology, Xi'an, 710054, People's Republic of China

<sup>2</sup>Department of Physics, Fudan University, Shanghai, 200433, People's Republic of China



(Received 14 October 2023; accepted 28 March 2024; published 17 April 2024)

The regulation of thermal transport is a challenging topic in complex networks. At present, the hidden physical mechanism behind thermal transport is poorly understood. This paper addresses this issue by proposing a complex network model that focuses on the thermal transport regulation through the manipulation of the network's degree distribution and clustering coefficient. Our findings indicate that increasing the degree distribution regulation parameter  $\sigma$  leads to reduced phonon localization and improved thermal transport efficiency. Conversely, increasing the clustering coefficient  $c$  results in enhanced phonon localization and reduced thermal transport efficiency. Meanwhile, by calculating the pseudodispersion relation of the network, we find that the maximum (or the second smallest) eigenfrequency decreases with increasing  $\sigma$  (or  $c$ ). Finally, we elucidate that phonon localization plays a pivotal role in the thermal transport of the network, as demonstrated through density of states and the participation ratio.

DOI: [10.1103/PhysRevE.109.044311](https://doi.org/10.1103/PhysRevE.109.044311)

### I. INTRODUCTION

As is well known, the field of thermal transport has consistently been a focal point of research and innovation. On the one hand, significant strides have been taken in this domain, aiming to enhance control over heat flux and mitigate thermal management challenges to a certain extent [1–6]. Concurrently, as research in this area has intensified, noteworthy thermally conductive materials have emerged, including thermally conductive silicone rubber [7], thermal interface materials [8], graphene [9], thermal insulating material [10], nanowires and nanotubes [11], and more.

On the other hand, complex networks have experienced comprehensive and profound development across diverse disciplines and fields, encompassing domains such as neuronal networks [12], biological networks [13], and nanotube and nanowire networks [14]. Notably, nanowires have garnered significant research attention in materials science and nanotechnology owing to their distinctive physical and chemical properties [15,16]. In the contemporary technological landscape, the emergence of nanowire nanojoining technology presents a captivating opportunity to craft intricate networks at the nanoscale [17–20]. This cutting-edge approach involves techniques such as nanowelding and nanofolding to establish nanojunctions. Consequently, it becomes imperative to develop models for these nanonetworks, scrutinize their thermal transport characteristics, and delve into the mechanisms underpinning these properties.

Presently, significant strides have been taken in the study of thermal transport within complex networks. For instance, it has been recognized that alterations to the network topology impact thermal transport, encompassing aspects such as node degree [21], degree correlation [22], and the self-organization of carbon nanotubes [23]. Furthermore, these changes can give rise to novel phenomena, such as interface thermal

resistance [24], thermal rectification [25], thermal siphon [26], and the vortex ratchet heat flow phenomenon [27]. However, despite these advances in controlling heat flux, the underlying physical mechanisms have remained largely unexplored. Therefore, there is an urgent need to gain a deeper understanding of the thermal transport properties within complex networks. It is well known that phonon localization can exert a significant influence on thermal transport in low-dimensional systems [28–30]. Nevertheless, the exploration of phonon localization in network structures has been limited, primarily due to the absence of translational invariance resulting from network structural disorder, which renders the conventional dispersion relation inapplicable to our model, making the study of phonon localization for thermal transport in complex networks a challenging endeavor.

Motivated by these challenges, we have undertaken a comprehensive investigation using a general network model to gain insights into the impact of clustering coefficient and degree distribution on thermal transport modes. Our findings reveal that network topology exerts a profound influence on thermal transport, with thermal transport efficiency decreasing as clustering coefficient  $c$  increases and as the parameter  $\sigma$  decreases. Furthermore, we have observed a significant influence of parameter  $\sigma$  and clustering coefficient  $c$  on the temperature distribution within complex networks. Specifically, an increase in parameter  $\sigma$  results in a progressively narrower temperature distribution, indicating a reduction in thermal resistance on each network edge. Conversely, an increase in clustering coefficient  $c$  leads to a progressively wider temperature distribution, signifying an increase in thermal resistance on each edge. Most importantly, we have conducted calculations to derive a pseudodispersion relation by computing the eigenvalues of the Laplacian matrix. Subsequently, we have determined the density of states and the participation ratio of the network. The results fully support the above simulation results, thus elucidating that phonon localization plays a pivotal role in regulating thermal transport within the network.

\*xiongkezhao@outlook.com

The subsequent sections of this paper are organized as follows. In Sec. II, we present the thermal transport model of the network we have constructed, elucidating its Hamiltonian, potential, dynamic equations, and other pertinent details. In Sec. III, we present the results of our numerical simulations, showcasing the thermal transport efficiency and the corresponding thermal resistance of the network across various parameter settings. Section IV offers insights into the underlying mechanisms shaping our numerical simulation results, with a particular emphasis on the role of phonon localization. This is elucidated through an analysis of the density of states and the participation ratio of the network. Finally, in Sec. V, we summarize our primary findings and provide a comprehensive discussion of the implications and future directions of our research.

## II. MODEL

Over the past two decades, the study of complex networks has witnessed significant advancements, leading to the development of various network models [31–33]. Among them, Erdős-Rényi (ER) networks and Barabasi-Albert (BA) scale-free networks [32] stand out as two typical examples. Notably, these two models exhibit distinct differences in their degree distributions. In the case of random networks, the degree distribution follows a binomial distribution, typically represented as  $P(k) \sim e^{-k}$ , while the BA model exhibits a power-law degree distribution, often expressed as  $P(k) \sim k^{-\gamma}$ , where  $k$  denotes the number of connections for each node.

In this study, we employ a generalized network model that offers flexibility with varying structures, ranging from random to scale-free, by adjusting the parameter  $\sigma$  [34]. The construction process for this generalized network model is as follows: Initially,  $m$  nodes are taken as initial nodes and each node is made to have  $m$  connected edges. Subsequently, at each time step, a new node is introduced. The  $m$  connected edges of the added nodes connect  $m$  existing nodes with probability  $\prod_i \sim (1 - \sigma)k_i + \sigma$ , where  $k_i$  is the degree of node  $i$  at that time, with the parameter  $0 \leq \sigma \leq 1$ , and a network with an average degree  $\langle k \rangle = 2m$  is generated after a long time of evolution. It should be emphasized that  $(1 - \sigma)k_i$  in  $\prod_i$  denotes preferred connections and  $\sigma$  in  $\prod_i$  denotes random connections. The degree distribution follows  $P(k) \sim [k + \sigma/(1 - \sigma)]^{-\gamma}$  [34], where the scaling exponent  $\gamma = 3 + \sigma/[m(1 - \sigma)]$ . Therefore, the degree distribution of the generated network will satisfy the power law  $P(k) \sim k^{-\gamma}$  for  $\sigma = 0$ , that is, the scale-free network; the degree distribution of the generated network satisfies the Poisson distribution  $P(k) \sim e^{-k/m}$  for  $\sigma = 1$ , that is, random network; the network presents a complex structure between a random network and a scale-free network when  $0 < \sigma < 1$ .

In addition, the change of clustering coefficient values has a significant effect on the topological patterns of complex networks. When clustering coefficient is small, it indicates the lower probability that the neighbors of a node are also connected with each other, as shown in Fig. 1(a). Conversely, when clustering coefficient is large, it indicates the higher probability that the neighbors of a node are also connected with each other, as shown in Fig. 1(b). Therefore, the topology of a network with a fixed degree distribution  $P(k)$  can be

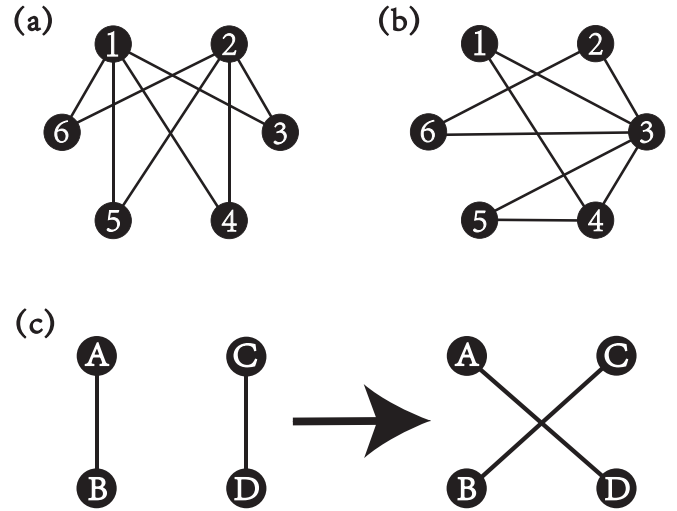


FIG. 1. The influence of network topology on clustering coefficient. In the network with six nodes and eight edges, (a) and (b) are network structures of low clustering coefficient 0 and high clustering coefficient 0.83, respectively. (c) Kim's reconnection method: randomly select two edges  $A-B$  and  $C-D$  each time in the original network, then delete the two edges  $A-B$  and  $C-D$ , and create two new edges  $A-D$  and  $B-C$ .

further modulated by manipulating its clustering coefficient, which denoted as  $c$ , it is defined as [35]:

$$c = \frac{1}{N} \sum \frac{2E_i}{k_i(k_i - 1)}, \quad (1)$$

where  $E_i$  is the number of edges actually connected between the  $k_i$  neighbors of node  $i$ . To modulate the clustering coefficient  $c$ , we utilize Kim's reconnection method [36], and implement an annealing algorithm [37] to get the maximum (or minimum) clustering coefficient within the network. The process unfolds as follows: First, set the parameter  $\sigma$  to generate a complex network with an average degree  $\langle k \rangle = 6$ . Second, randomly select two edges, one connecting node  $A$  and  $B$ , and the other connecting node  $C$  and  $D$ . By making each node change partners, the original edges  $A-B$  and  $C-D$  cease to exist and are replaced by new edges  $A-D$  and  $B-C$ , as illustrated in Fig. 1(c). Note that duplicate edges are avoided during the reconnection process. Following such cross edging, the degree of each node does not change, so the degree distribution of the whole network nodes remain unchanged. Furthermore, this approach preserves the essential properties of the node. This ensures that certain pivotal nodes in the network maintain their significance from the original network even after the reconstruction [36]. Next, check whether the new connections lead to an increase (or decrease) in the sum of clustering coefficient for the four nodes involved in the two connected edges. If so, the operation is considered valid. Conversely, if this operation fails to increase (or decrease) the network's clustering coefficient, we introduce a minute probability parameter, denoted as  $f = 0.01$ , to determine whether to retain the aforementioned edge connection operation. Specifically, if a randomly generated number falls below  $f$ , the operation is preserved. Otherwise, if the random number exceeds  $f$ , the operation is abandoned, and the

edges remain unchanged, proceeding to the next iteration. This iterative process persists until the disparity between the global clustering coefficient and the desired clustering coefficient is less than  $10^{-3}$ . At this point, we consider that the target clustering coefficient has been achieved. This approach enhances the algorithm's likelihood of escaping local optima and increases the probability of reaching the target clustering coefficient. Leveraging this methodology, we can manipulate the degree distribution and clustering properties of the network, respectively, thereby enabling a comprehensive exploration of their impact on the network's thermal transport characteristics.

The study of thermal transport in networks typically employs the FPU model [38], and the potential energy of the FPU model is defined as

$$V(x) = \frac{g_2}{2}x^2 + \frac{g_3}{3}x^3 + \frac{g_4}{4}x^4. \quad (2)$$

This potential energy can be understood as arising from the expansion of  $V$  around its equilibrium position at  $x = 0$ . Specifically, for the case of  $g_4$  is equal to zero, the model is referred to as the FPU- $\alpha$  model; for the case of  $g_3$  is zero, the model is referred to as the FPU- $\beta$  model [39–41].

The Hamiltonian of the system is

$$H = \sum_{i=1}^N \left[ \frac{p_i^2}{2M_i} + U(x_i) + V_i(x_{i+1} - x_i) \right], \quad (3)$$

where  $i$  traverses all nodes of the network,  $i = 1, 2, \dots, N$ ,  $M_i$  represents the mass of the  $i$ th node,  $x_i$  represents the displacement from the equilibrium position of the  $i$ th node,  $U(x)$  denotes the substrate potential energy, in order to maintain the variables, we let  $U(x_i) = 0$  and only the interactions between the nearest-neighbor nodes are considered, therefore, the system potential energy can be expressed as

$$V_i(x_i) = \frac{1}{2} \sum_{j=1}^{k_i} \left[ \frac{1}{2}(x_i - x_j)^2 + \frac{\beta}{4}(x_i - x_j)^4 \right]. \quad (4)$$

For simplicity, we set  $M_i = 1$ . The thermostats are chosen as the common Nose-Hoover thermostats [42,43], and the dynamics of the source nodes satisfy

$$\begin{aligned} \dot{x}_h &= \frac{\partial H}{\partial p_h}, & \dot{p}_h &= -\frac{\partial H}{\partial x_h} - \xi_h p_h, \\ \dot{x}_l &= \frac{\partial H}{\partial p_l}, & \dot{p}_l &= -\frac{\partial H}{\partial x_l} - \xi_l p_l. \end{aligned} \quad (5)$$

The dynamic equations of the thermostats satisfy

$$\begin{aligned} \dot{\xi}_h &= \frac{\dot{x}_h}{T_h} - 1, \\ \dot{\xi}_l &= \frac{\dot{x}_l}{T_l} - 1. \end{aligned} \quad (6)$$

Except for the source nodes, the motions of all other nodes in the network obey the canonical equations

$$\begin{aligned} \dot{x}_i &= \frac{\partial H}{\partial p_i}, \\ \dot{p}_i &= -\frac{\partial H}{\partial x_i}. \end{aligned} \quad (7)$$

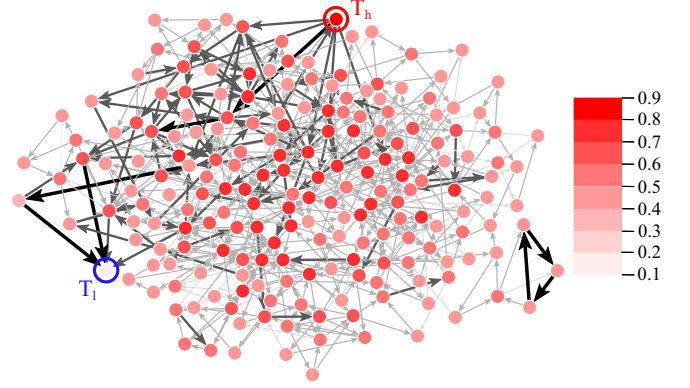


FIG. 2. Schematic diagram of heat flux distribution and node temperature distribution in a random network. The solid red circle represents the node, and its color depth represents the temperature. The node surrounded by the red (blue) circle is connected to the thermostat with the high temperature  $T_h$  (low temperature  $T_l$ ). The arrows represent the direction of heat flux at steady state, and their darker color means a larger heat flux. Here the size of the network  $N = 200$  and the average degree  $\langle k \rangle = 6$ .

It should be emphasized that the dynamics simulation in this study employs the fourth-order Runge-Kutta algorithm with an integration time step of 0.01, and after a transient process of time  $10^6$ , the thermal transport within the network reaches a steady state. The local temperature of node  $i$  can be defined as [39,40]

$$T(i) = \left\langle \frac{p_i^2}{M_i} \right\rangle. \quad (8)$$

The heat flux at the edge between neighboring nodes  $i$  and  $j$  can be calculated by the following equation:

$$J_{ij} = \langle \dot{x}_i \partial V / \partial x_j \rangle, \quad (9)$$

where  $\langle \cdot \cdot \cdot \rangle$  is the long time average, which takes the value of  $10^7$  in this study.

### III. NUMERICAL SIMULATION

In the numerical simulation, we consider a network size of  $N = 200$  nodes with an average degree of  $\langle k \rangle = 6$ , and randomly select two nodes in the network as the high- and low-temperature source nodes connected to the Nose-Hoover thermostat [42,43]. Fixed boundary conditions are applied to the source nodes. The temperatures of the thermostats are set as  $T_h = 0.9$  and  $T_l = 0.1$ , respectively, as illustrated in Fig. 2. We define  $J$  as the total heat flux in the network, with its magnitude serving as a measure of heat transport efficiency, which is calculated as the sum of heat flux from the high-temperature source node  $i_0$  to all its neighboring nodes, or as the sum of heat flux from the network to the low-temperature source node  $j_0$ . This can be expressed as [44]

$$J = \sum_{j=1}^{k_{i_0}} J_{i_0 j}. \quad (10)$$

After the transient process,  $J$  will stabilize.

To elucidate the impact of the degree-distribution regulation parameter  $\sigma$  and the clustering regulation parameter  $c$  on

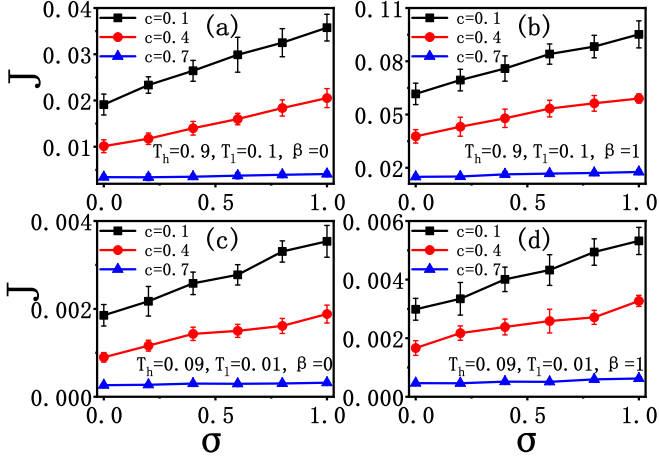


FIG. 3. Effect of parameter  $\sigma$  on the total heat flux  $J$  of the network. (a) and (b) illustrate the variation of total network heat flux  $J$  with parameter  $\sigma$ , where  $T_h = 0.9$  and  $T_l = 0.1$ , at  $\beta$  values of 0.0 and 1.0, respectively. (c) and (d) illustrate the variation of total network heat flux  $J$  with parameter  $\sigma$ , where  $T_h = 0.09$  and  $T_l = 0.01$ , at  $\beta$  values of 0.0 and 1.0, respectively. Black squares, red circles and blue triangles represent the cases of clustering coefficient  $c = 0.1, 0.4$ , and  $0.7$ , respectively.

thermal transport, we conducted an extensive series of numerical simulations for networks with different parameters  $\sigma$  and different clustering coefficients  $c$  at different  $\beta$  values. Specifically, we considered  $\beta$  values of 0 [Fig. 3(a)] and 1 [Fig. 3(b)] for the cases of  $T_h = 0.9$  and  $T_l = 0.1$ . It is evident from the results that the total heat flux  $J$  monotonically increases as  $\sigma$  increases. This suggests that random networks are more conducive to thermal transport to scale-free networks. In order to further explore the influence of thermostats' temperatures on this characteristic, we research the dependence of the total heat flux  $J$  for the case of  $T_h = 0.09$  and  $T_l = 0.01$ . The outcomes presented in Figs. 3(c) and 3(d) affirm that the total heat flux  $J$  monotonically increases as  $\sigma$  increases. Thus the change of the thermostat temperatures do not alter the conclusion that random networks are conducive for the thermal transport.

Next we further explored the variation of the total heat flux  $J$  with different clustering coefficients  $c$  where  $\beta$  values are taken as 0 [Fig. 4(a)] and 1 [Fig. 4(b)] for the cases of  $T_h = 0.9$  and  $T_l = 0.1$ , respectively. As the clustering coefficient  $c$  increases,  $J$  monotonically decreases. Notably, the curve with  $\sigma = 1$  exhibits the most significant reduction, while the curve with  $\sigma = 0$  displays the smallest reduction. This implies that larger values of  $c$  is less conducive for the thermal transport in the network and larger values of  $\sigma$  promote the thermal transport within the network. In our pursuit of a deeper understanding of the impact of thermostat temperatures on this characteristic, we investigated the dependency of the total heat flux  $J$  under different thermostat temperatures, specifically  $T_h = 0.09$  and  $T_l = 0.01$ . The outcomes presented in Figs. 4(c) and 4(d) affirm that the total heat flux  $J$  monotonically decreases as  $c$  increases. Thus the change of the thermostat temperatures do not alter the conclusion that larger values of  $c$  is less conducive for the thermal transport.

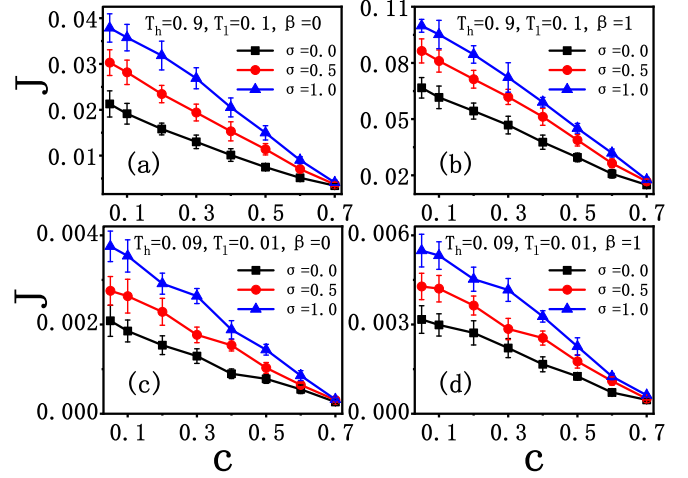


FIG. 4. Effect of clustering coefficient  $c$  on the total heat flux  $J$  of the network. (a) and (b) illustrate the variation of the total network heat flux  $J$  with the clustering coefficient  $c$ , where  $T_h = 0.9$  and  $T_l = 0.1$ , at  $\beta$  values of 0.0 and 1.0, respectively. (c) and (d) illustrate the variation of the total network heat flux  $J$  with the clustering coefficient  $c$ , where  $T_h = 0.09$  and  $T_l = 0.01$ , at  $\beta$  values of 0.0 and 1.0, respectively. Black squares, red circles, and blue triangles represent the cases of  $\sigma = 0.0, 0.5$ , and  $1.0$ , respectively.

In order to explore whether the average degree of the network has an effect on the above-mentioned thermal transport, we carried out a large number of numerical simulations of the thermal transport of the network with different degree distribution control parameters  $\sigma$  and cluster coefficients  $c$ . Figures 5(a)–5(c) show the dependence of the total heat flux  $J$  on the parameter  $\sigma$  for  $c = 0.1, 0.4$ , and  $0.7$ , respectively, where  $\beta = 1$ , squares and circles represent the network when the average degree  $\langle k \rangle = 6$  and  $10$  of the network, respectively. As can be seen from the figure, when the average degree is large, the change of parameter  $\sigma$  has little influence on the heat flux, because the randomness of the network is weakened when the average degree is large.

Figures 6(a)–6(c) show the dependence of total heat flux  $J$  on the cluster coefficient  $c$  of degree distribution when  $\sigma = 0.0, 0.5$  and  $1.0$  where  $\beta$  values are taken as 1, respectively, squares and circles represent the network when the average degree  $\langle k \rangle = 6$  and  $10$ , respectively. We observe that the average degree of the network does not alter the

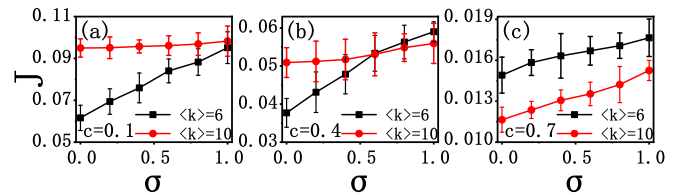


FIG. 5. Effect on the total heat flux  $J$  of the network after changing parameter  $\sigma$  for different average degrees. (a)–(c) illustrate the variation of the total network heat flux  $J$  with parameter  $\sigma$  for  $c = 0.1, c = 0.4$ , and  $c = 0.7$  under different average degrees, respectively. Black squares and red circles represent the cases of  $\langle k \rangle = 6$  and  $10$ , respectively.

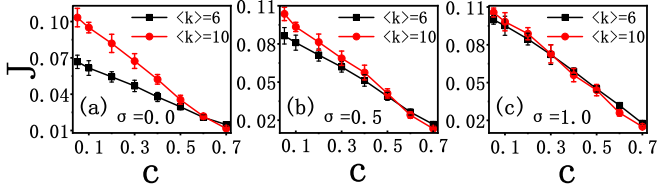


FIG. 6. Effect on the total heat flux  $J$  of the network after changing clustering coefficient  $c$  for different average degrees. (a)–(c) illustrate the variation of the total network heat flux  $J$  with the clustering coefficient  $c$  for  $\sigma = 0.0$ ,  $\sigma = 0.5$ , and  $\sigma = 1.0$  under different average degrees respectively. Black squares and red circles represent the cases of  $\langle k \rangle = 6$  and  $10$ , respectively.

conclusion regarding the impact of the aforementioned clustering coefficient  $c$  on thermal transport.

Additionally, when we maintained a fixed clustering coefficient  $c = 0.1$  [Figs. 7(a)–7(d)], the temperature distribution progressively narrowed as the parameter  $\sigma$  increased. This suggests that with larger values of  $\sigma$ , the temperatures of most nodes in the network tend to approach uniformity. In order to understand the mechanism of these significant differences, we further investigated the variation of thermal resistance, which can be expressed by the following equation [24]:

$$R_{ij} = \frac{\Delta T_{ij}}{J_{ij}}, \quad (11)$$

where  $\Delta T_{ij}$  denotes the temperature difference between two neighboring nodes  $i$  and  $j$  and  $J_{ij}$  is the same as the representation in Eq. (10), which denotes the heat flux transferred between two neighboring nodes  $i$  and  $j$ .

It is worth noting that higher values of thermal resistance signify greater hindrance to heat transfer, leading to slower efficiency of thermal transport. Conversely, lower thermal resistance facilitates faster thermal transport efficiency. We show in Figs. 7(e)–7(h) the relationship between the change in thermal resistance of each edge for  $\sigma = 0.0, 0.3, 0.7$ , and  $1.0$ , respectively. As  $\sigma$  increases, the probability of connection between nodes increases and the connections in the network are more uniform. Consequently, larger values of  $\sigma$  lead to reduced thermal resistance on each edge, making heat transfer more efficient between nodes. The smaller loss of heat transfer

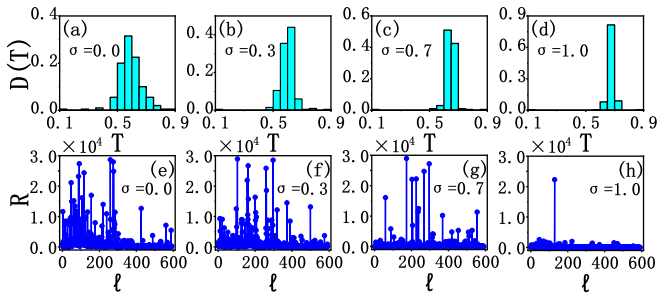


FIG. 7. Nodes temperature distribution and thermal resistance of each edge. (a)–(d) are the distribution  $D(T)$  of nodes temperature  $T$  for different parameters  $\sigma = 0.0, 0.3, 0.7$ , and  $1.0$  for clustering coefficient  $c = 0.1$ , respectively. (e)–(h) are the values of thermal resistance corresponding to each edge for different parameters  $\sigma = 0.0, 0.3, 0.7$ , and  $1.0$  for clustering coefficient  $c = 0.1$ , respectively.

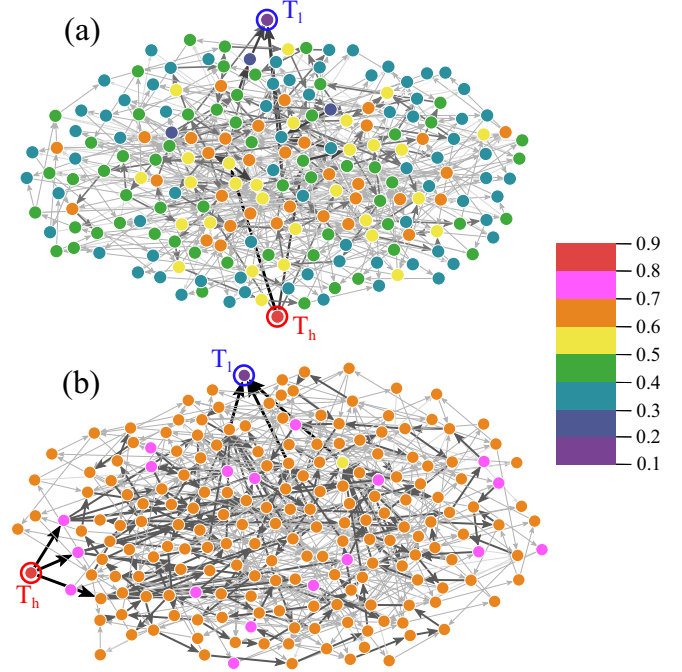


FIG. 8. Heat flux and nodes temperature distribution in network. (a) and (b) are heat flux distribution with average degree  $\langle k \rangle = 6$  for  $\sigma = 0$  and  $1$ , respectively. The difference in node color represents the difference in temperature. The nodes surrounded by red (blue) circles are connected to the thermostat with the high temperature  $T_h$  (low temperature  $T_l$ ). The arrows represent the direction of heat flux at steady state, and their darker color means a larger heat flux.

in the network reduces the temperature difference between nodes and contributes to a relatively narrow temperature distribution within the network.

Next, we visualize the above results in Fig. 8. Figures 8(a) and 8(b) show the heat flux on the network and the temperature distribution among the nodes for the parameters  $\sigma = 0.0$  and  $1.0$ , respectively, which illustrate that as the degree distribution regulation parameter  $\sigma$  increases, the heat flux increases, and the temperature distribution tends to be consistent, which is consistent with the results we discussed above.

Similarly, we fix the parameter  $\sigma = 1.0$ , and vary the clustering coefficient  $c$  [Figs. 9(a)–9(d)], we observe that the temperature distribution gradually widens as the clustering coefficient  $c$  increases. This indicates that larger values of  $c$  result in a broader range of temperature distribution among the nodes in the network, which can be similarly interpreted in terms of thermal resistance [Figs. 9(e)–9(h)]. When the clustering coefficient  $c$  increases, it means that denser connections are formed between the nodes in the network and the aggregation of nodes increases, which results in increasing heat transfer losses. Consequently, the thermal resistance on each edge rises, leading to greater hindrance to thermal transport. This, in turn, results in larger temperature differences between nodes. In other words, the wider the temperature differences between nodes, the broader the temperature distribution across the network.

We then visualize the above results in Fig. 10. Figures 10(a) and 10(b) show the heat flux and the temperature distribution

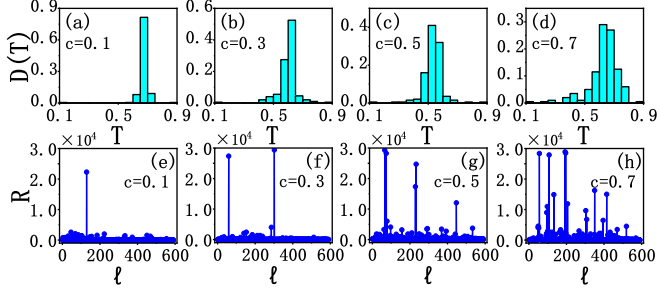


FIG. 9. Nodes temperature distribution and thermal resistance of each edge. (a)–(d) are the distribution  $D(T)$  of nodes temperature  $T$  for different clustering coefficients  $c = 0.1, 0.3, 0.5,$  and  $0.7$  for parameter  $\sigma = 1.0$ . (e)–(h) are the values of thermal resistance corresponding to each edge for different clustering coefficients  $c = 0.1, c = 0.3, c = 0.5,$  and  $c = 0.7$  for parameter  $\sigma = 1.0$ , respectively.

on the nodes for clustering coefficient  $c = 0.1$  and  $0.7$  on the random network, respectively. These visualizations illustrate that with a larger clustering coefficient, the heat flux decreases, and the range of temperature distribution becomes wider, which is in line with the results we discussed above.

#### IV. PHONON LOCALIZATION

In order to explore the mechanism behind the simulation results in Sec. III, we introduce the pseudodispersion relation of the general network structure to elucidate the observed

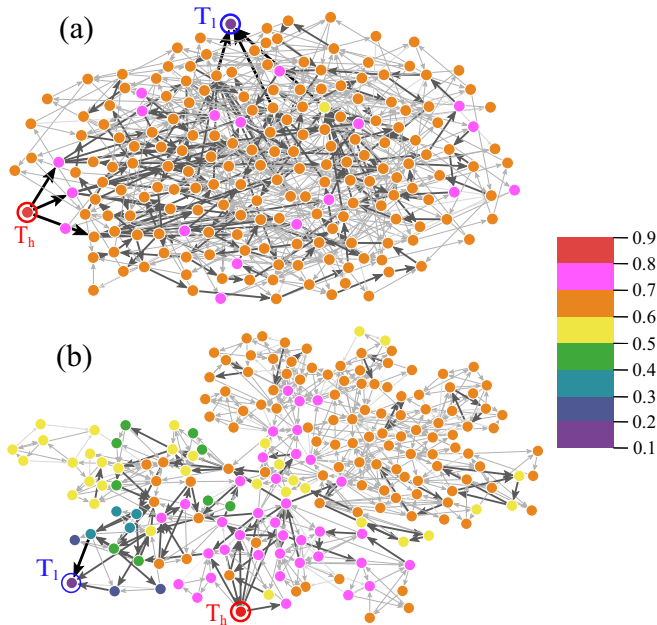


FIG. 10. Heat flux and nodes temperature distribution in network. (a) and (b) are heat flux distribution with average degree  $\langle k \rangle = 6$  and  $\sigma = 1$  for clustering coefficient  $c = 0.1$  and  $0.7$ , respectively. In these visualizations, variations in node color indicate differences in temperature. Nodes encircled by red (blue) circles are linked to the thermostat with high temperature  $T_h$  (low temperature  $T_l$ ). The arrows represent the direction of heat flux at steady state, and their darker color means a larger heat flux.

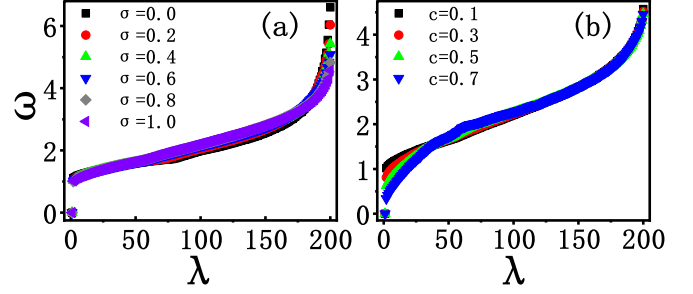


FIG. 11. The influence of parameter  $\sigma$  and  $c$  on the pseudo-dispersion relation. (a) The eigenfrequency  $\omega$  versus its eigenmode index  $\lambda$  of random networks for  $\sigma = 0.0, 0.2, 0.4, 0.6, 0.8,$  and  $1.0$ , respectively. (b) The eigenfrequency  $\omega$  versus its eigenmode index  $\lambda$  of networks for  $c = 0.1, 0.3, 0.5,$  and  $0.7$ , respectively.

outcomes [45]. First, by substituting Eq. (3) into (7), we obtain

$$\ddot{u}_i = \sum_{j=1}^{k_i} (u_j - u_i) + \frac{\beta}{2} (u_j - u_i)^3. \quad (12)$$

Decomposing the amplitude  $u_i$  in the above equation into the eigenvector  $e_{\omega,i}$  with eigenmodes  $e_{\omega}$

$$u_i = \sum_{\omega} Q_{\omega} e_{\omega,i}, \quad (13)$$

where  $Q_{\omega}$  is a time-dependent expansion coefficient with the expression  $Q_{\omega}(t) = \exp(-i\omega t)$ . Then Eq. (12) can be simplified as

$$-\omega^2 e_{\omega} = G \cdot e_{\omega}, \quad (14)$$

where the matrix  $G$  represents the coupling interactions of neighboring nodes and the  $N \times N$  matrix  $G$  can be expressed as

$$G_{i,j} = X_{i,j} - I_{i,j}, \quad (15)$$

where matrix  $X$  denotes the adjacency matrix in the network. If there is a connecting edge between node  $i$  and node  $j$ , then  $X(i, j) = 1$ , otherwise  $X(i, j) = 0$ . The matrix  $I$  is a diagonal matrix denoted as  $I_{i,j} = \delta_{i,j} k_i$ .

Figure 11(a) shows the eigenfrequency  $\omega$  versus its eigenmode index  $\lambda$  for a general network with different parameters  $\sigma = 0.0, 0.2, 0.4, 0.6, 0.8,$  and  $1.0$  for clustering coefficient  $c = 0.1$ . Variation of the parameter  $\sigma$  significantly perturbs the pseudodispersion relation of the network, specifically, for the same eigenmode index  $\lambda$ , the maximum eigenfrequency (cutoff frequency)  $\omega_{\max} = \omega_{\lambda=200}$  monotonically decreases as  $\sigma$  increases, as shown in Fig. 11(a). This implies that the degree distribution influences the extent of distribution of vibration modes within the network.

Similarly, we investigated the pseudodispersion relation for different clustering coefficients under random networks. Figure 11(b) shows the eigenfrequency  $\omega$  versus its eigenmode index  $\lambda$  for random networks with different clustering coefficients  $c = 0.1, 0.3, 0.5,$  and  $0.7$ . Variations in the clustering coefficient  $c$  perturb the pseudodispersion relation of the network. Specifically, for the same eigenmode index  $\lambda$ , the second smallest eigenvalue decreases with increasing clustering coefficient  $c$ , as shown in Fig. 11(b). This implies

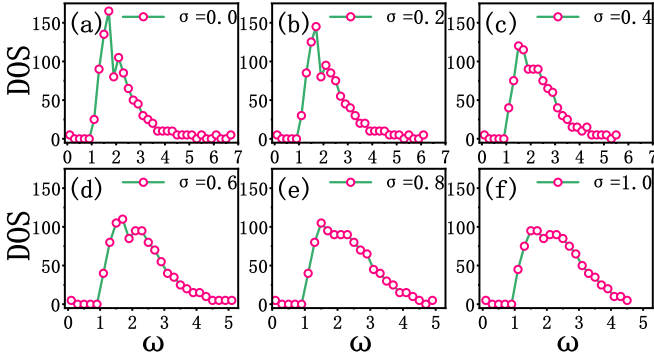


FIG. 12. Phonon density of states for different parameters  $\sigma$  of size  $N = 200$ . (a)–(f) are the DOS of a network for  $\sigma = 0.0, 0.2, 0.4, 0.6, 0.8,$  and  $1.0$ , respectively.

that the clustering coefficient also has an effect on the distribution range of the vibration modes. We all know that the variation of the second smallest eigenvalue can have an effect on epidemic spread [46], system synchronization [47], etc., and we find here for the first time that the variation of the second smallest eigenvalue can also have an effect on thermal transport.

In order to more accurately analyze the variation of the pseudodispersion relation in Fig. 11 and to further understand the properties of phonon vibrations, we introduce the phonon density of states, which is defined as [48]

$$g(\omega) = \sum_{\Delta\omega \rightarrow 0} \frac{\Delta n}{\Delta\omega}. \quad (16)$$

We further investigate the density of states (DOS) of the parameter  $\sigma$  and the clustering coefficient  $c$ . We know that the DOS spikes are often referred to as van Hove singularity, which indicates the transition between different vibrational modes. By adjusting the parameter  $\sigma$  and the clustering coefficient  $c$ , we can observe changes in the position and shape of the spikes in the DOS. The positions of these spikes can correspond to specific vibrational patterns, and changes in their shapes can reveal interactions between variations in network structure and vibrational patterns. Figure 12 shows the DOS for different parameters  $\sigma$ , which can be regarded as the inverse of the derivative of the curve shown in Fig. 11(a). It can be clearly seen that in Fig. 12, as the parameter  $\sigma$  increases, the spikes gradually weaken and eventually disappear. Figure 13 shows the DOS for different clustering coefficients  $c$  under the random network, and it can be seen that the spikes gradually appear as the clustering coefficient  $c$  increase. These changes in the DOS provide valuable insights into the relationship between network parameters and vibrational patterns.

We further introduce the participation ratio (PR) to quantify the strength of localization of different vibrational modes [49,50]

$$P_\omega = \frac{1}{N \sum_i (e_{i,\omega}^* e_{i,\omega})^2}, \quad (17)$$

where  $N$  is the number of phonon occupancies given by the Bose-Einstein distribution and  $e_{\omega,i}$  is the eigenvector

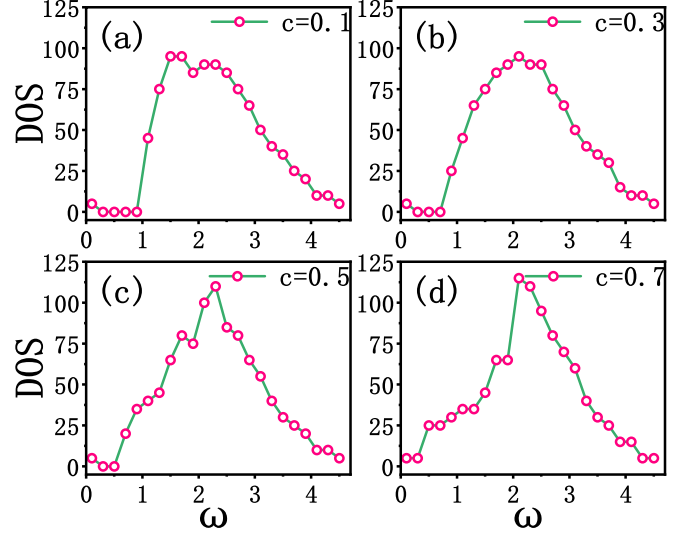


FIG. 13. Phonon density of states for different clustering coefficients  $c$  of size  $N = 200$ . (a)–(d) are the DOS of a network for  $c = 0.1, 0.3, 0.5,$  and  $0.7$ , respectively.

component of the eigenvalue  $\omega$ . For a perfect extended state we have  $P = 1$ , while for a state strongly localized on one node it tends to  $1/N$  [49]. Thus, the PR provides a measure of the extent to which the vibrational modes are spatially distributed; a large PR indicates that the modes have a broad spatial distribution, while a small PR indicates that the modes are localized. We show the PR of vibrational modes in general networks as a function of the eigenfrequency  $\omega$  of various degree distribution modulation parameter  $\sigma$  and clustering coefficient  $c$ . These results demonstrate that the structural properties of the network influence the spatial distribution of vibrational modes, subsequently affecting the intensity of localization within the network.

Figure 14 illustrates the PR of the vibrational modes in the general network as a function of the eigenfrequency  $\omega$  of the various parameters  $\sigma$ . It can be clearly seen that the variation of the parameter  $\sigma$  has an impact on the localized intensity. Specifically, as the parameter  $\sigma$  increases, the

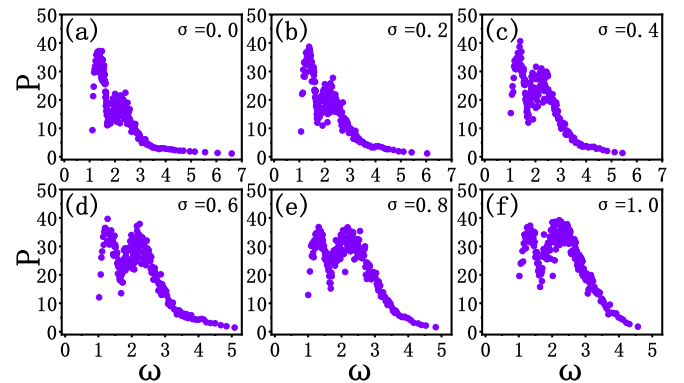


FIG. 14. Eigenmode participation ratio of generalized networks vs. the eigenfrequency,  $\omega$ , for different  $\sigma$ : (a)  $\sigma = 0.0$ , (b)  $\sigma = 0.2$ , (c)  $\sigma = 0.4$ , (d)  $\sigma = 0.6$ , (e)  $\sigma = 0.8$ , and (f)  $\sigma = 1.0$ . Simulation data for spring networks with  $n = 200$  and  $M = 1$ .

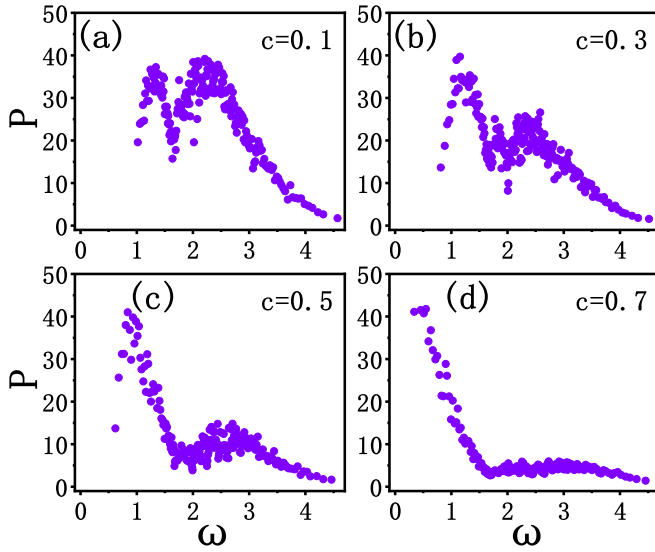


FIG. 15. Eigenmode participation ratio of generalized networks vs. the eigenfrequency,  $\omega$ , for different  $c$ : (a)  $c = 0.1$ , (b)  $c = 0.3$ , (c)  $c = 0.5$ , and (d)  $c = 0.7$ . Simulation data for spring networks with  $n = 200$  and  $M = 1$ .

PR of the high-frequency part increases continuously, which means that the extended mode predominates. The value of PR for regions  $\omega > 1$  is initially smaller and increases with increasing  $\sigma$ , which implies that the vibrational modes are transitioning from localized states to extended states. Figure 15 shows the PR of the vibrational modes in the random network as a function of the eigenfrequency  $\omega$  for various clustering coefficient  $c$ . As the clustering coefficient  $c$  increases, we can see that the PR for the high-frequency part of the network keeps decreasing, which implies that localized modes predominate. Illustrated in Fig. 14(a), the participation ratio exhibits two distinct peaks, suggesting the presence of two van Hove singularities. This indicates a transition from the local state  $\rightarrow$  the extended state  $\rightarrow$  the local state  $\rightarrow$  the extended state  $\rightarrow$  the local state, resulting in the observation of double peaks in Fig. 12(a). Figure 15(a) emphasizes this observation, depicting the occurrence of double peaks when the parameter  $c = 0.1$ . Nevertheless, as  $c$  increases, one of the peaks diminishes and eventually disappears in Fig. 15(d), signifying a transition from the local state  $\rightarrow$  the extended state  $\rightarrow$  the local state, resulting in the observation of only single peak in Fig. 13(d). Therefore, under these conditions, the corresponding density of states behaves unimodally. It is widely known that phonon localization hinders the transport of energy. By assessing the degree of phonon localization using the participation ratio, we can deduce that as the parameter  $\sigma$  increases, phonon localization becomes weaker. As a result, thermal transport efficiency improves, leading to an increase in heat flux at the network's edges. This, in turn, reduces thermal resistance and narrows the temperature distribution among network nodes. Conversely, when the clustering coefficient  $c$  increases, phonon localization becomes more pronounced, causing a decrease in thermal transport efficiency. This weakens the heat flux at the connecting edges of the network, leading to higher thermal resistance and a broader temperature distribution among network nodes.

## V. CONCLUSION AND DISCUSSION

We employed a generalized network model to investigate the influence of the degree distribution modulation parameter  $\sigma$  and the clustering coefficient  $c$  on thermal transport within the network. Our findings reveal that as the clustering coefficient  $c$  increases, the thermal transport efficiency of the network decreases and, accordingly, the thermal resistance of each edge increases. Conversely, as the parameter  $\sigma$  increases, the thermal transport efficiency of the network subsequently increases and the thermal resistance of each edge decreases. Most significantly, we elucidate the physical mechanisms by which both the degree distribution and clustering coefficient influence the thermal transport within the network through calculations of the pseudodispersion relation, states density, and the phonon participation ratio. Specifically, with the increase of parameter  $\sigma$ , the state density spikes gradually diminish, and the PR in the high-frequency part increases, indicating that the vibrational modes are transitioned from localized states to extended states. Conversely, with the increase of the clustering coefficient  $c$ , the state density spikes gradually strengthen, and the PR in the high-frequency part decreases, indicating that the vibrational modes are transitioned from extended states to localized states. Therefore, phonon localization will affect the thermal transport efficiency of the network. With the weakening of phonon localization, the thermal transport efficiency of the network increases. On the flip side, with the enhancement of phonon localization, the thermal transport of the network decreases.

The above theoretical results are consistent with some experimental results. For example, it has been demonstrated in experiments measuring the thermal conductivity of ultrathin single-walled carbon nanotube networks that the thermal transport properties of carbon nanotube networks are extremely sensitive to the intertube junctions of the nanotubes [51,52]. Moreover, it has been shown in experiments measuring the thermal conductivity of random networks of three-dimensional carbon nanotubes that the coefficient of thermal conductivity of double junctions at room temperature is about an order of magnitude smaller than that of single junctions [53], which is consistent with our theoretical result that the network thermal transport increases with the increase of the degree distribution regulation parameter  $\sigma$ . Because when the parameter  $\sigma$  increases, the number of nodes with a higher count of cross-connected edges decreases. In addition, the clustering coefficient  $c$  represents the probability that the neighbors of nodes are also connected to each other, corresponding to the aggregation behavior of nanoparticles in the experiment. The latest research in experiments indicates that the thermal conductivity of composites will decrease with the increase of particle aggregation concentration [54,55], which is consistent with our theoretical result that the network thermal transport decreases with the increase of the clustering coefficient  $c$ . This greatly enhances the credibility of our conclusions.

In summary, we establish a fundamental link between network topology and system eigenfrequencies, offering a theoretical foundation for understanding the vibrational characteristics of networks. We have shown that for the same eigenmode index  $\lambda$ , the maximum cutoff frequency  $\omega_{\max}$



decreases with the increase of the degree-distribution modulation parameter  $\sigma$ , and the second smallest eigenvalue decreases with the increase of the clustering coefficient  $c$ , indicating that the strength of localization in a complex network can be manipulated by adjusting the topology of the network. In this way, thermal transport can be controlled by tuning the structural or vibrational properties of the network, enabling the optimization of thermal performance. These findings are of great significance for the development of strategies to regulate thermal transport for complex networks and provide

further exploration and development in the study of phonon localization in disordered networks.

### ACKNOWLEDGMENTS

We acknowledge financial support from the National Natural Science Foundation of China under Grants No. 12005166, and from the China Postdoctoral Science Foundation under Grants No. 2022M720036 and No. 2023T160110.

- 
- [1] N. Li, J. Ren, L. Wang, G. Zhang, P. Hänggi, and B. Li, *Rev. Mod. Phys.* **84**, 1045 (2012).
- [2] Y. F. Ding, G. M. Zhu, X. Y. Shen, X. Bai, and B. W. Li, *Chin. Phys. B* **31**, 126301 (2022).
- [3] A. L. Moore and L. Shi, *Mater. Today* **17**, 163 (2014).
- [4] W. Li, Y. Shi, Z. Chen, and S. Fan, *Nat. Commun.* **9**, 4240 (2018).
- [5] D. Dan, C. Yao, Y. Zhang, H. Zhang, Z. Zeng, and X. Xu, *Appl. Therm. Eng.* **162**, 114183 (2019).
- [6] A. Afzal, J. K. Bhutto, A. Alrobaian, A. Razak Kaladgi, and S. A. Khan, *Energies* **14**, 7370 (2021).
- [7] W. Y. Zhou, S. H. Qi, H. Z. Zhao, and N. L. Liu, *Polym. Composite.* **28**, 23 (2007).
- [8] D. D. L. Chung, *Appl. Therm. Eng.* **21**, 1593 (2001).
- [9] A. K. Geim, *Science* **324**, 1530 (2009).
- [10] A. M. Papadopoulos, *Energ. Buildings* **37**, 77 (2005).
- [11] R. Yan, D. Gargas, and P. Yang, *Nature Photon.* **3**, 569 (2009).
- [12] C. M. Bishop, *Rev. Sci. Instrum.* **65**, 1803 (1994).
- [13] E. Alm and A. P. Arkin, *Curr. Opin. Struct. Biol.* **13**, 193 (2003).
- [14] Y. Song, R. M. Garcia, R. M. Dorin, H. Wang, Y. Qiu, E. N. Coker, W. A. Steen, J. E. Miller, and J. A. Shelnut, *Nano Lett.* **7**, 3650 (2007).
- [15] R. H. Baughman, A. A. Zakhidov, and W. A. De Heer, *Science* **297**, 787 (2002).
- [16] M. Fujii, X. Zhang, H. Xie, H. Ago, K. Takahashi, T. Ikuta, H. Abe, and T. Shimizu, *Phys. Rev. Lett.* **95**, 065502 (2005).
- [17] Y. Peng, T. Cullis, and B. Inkson, *Nano Lett.* **9**, 91 (2009).
- [18] S. Dai, Q. Li, G. Liu, H. Yang, Y. Yang, D. Zhao, W. Wang, and M. Qiu, *Appl. Phys. Lett.* **108**, 193101 (2016).
- [19] X. Li, J. Lyu, C. Goldmann, M. Kociak, D. Constantin, and C. Hamon, *J. Phys. Chem. Lett.* **10**, 7093 (2019).
- [20] E. C. Garnett, W. Cai, J. J. Cha, F. Mahmood, S. T. Connor, M. Greyson Christoforo, Y. Cui, M. D. McGehee, and M. L. Brongersma, *Nature Mater.* **11**, 241 (2012).
- [21] K. Xiong, C. Zeng, Z. Liu, and B. Li, *Phys. Rev. E* **98**, 022115 (2018).
- [22] K. Xiong, C. Zeng, and Z. Liu, *Nonlinear Dyn.* **94**, 3067 (2018).
- [23] A. N. Volkov and L. V. Zhigilei, *Phys. Rev. Lett.* **104**, 215902 (2010).
- [24] Z. Liu and B. Li, *Phys. Rev. E* **76**, 051118 (2007).
- [25] Z. Liu, X. Wu, H. Yang, N. Gupte, and B. Li, *New J. Phys.* **12**, 023016 (2010).
- [26] K. Xiong, Z. Liu, C. Zeng, and B. Li, *Natl. Sci. Rev.* **7**, 270 (2020).
- [27] S. Wang, C. Zeng, G. Zhu, H. Wang, and B. Li, *Phys. Rev. Res.* **5**, 043009 (2023).
- [28] M. N. Luckyanova, J. Mendoza, H. Lu, B. Song, S. Huang, J. Zhou, and G. Chen, *Sci. Adv.* **4**, eaat9460 (2018).
- [29] S. Hu, Z. Zhang, P. Jiang, J. Chen, S. Volz, M. Nomura, and B. Li, *J. Phys. Chem. Lett.* **9**, 3959 (2018).
- [30] T. Zhu and E. Ertekin, *Phys. Rev. B* **93**, 155414 (2016).
- [31] S. Boccaletti, V. Latora, Y. Moreno, M. Chavez, and D. U. Hwang, *Phys. Rep.* **424**, 175 (2006).
- [32] A. L. Barabási and R. Albert, *Science* **286**, 509 (1999).
- [33] D. J. Watts and S. H. Strogatz, *Nature (London)* **393**, 440 (1998).
- [34] Z. Liu, Y. C. Lai, N. Ye, and P. Dasgupta, *Phys. Lett. A* **303**, 337 (2002).
- [35] R. Albert and A. L. Barabási, *Rev. Mod. Phys.* **74**, 47 (2002).
- [36] B. J. Kim, *Phys. Rev. E* **69**, 045101(R) (2004).
- [37] S. Kirkpatrick, C. D. Gelatt, and M. P. Vecchi, *Science* **220**, 671 (1983).
- [38] B. Hu, B. Li, and H. Zhao, *Phys. Rev. E* **57**, 2992 (1998).
- [39] S. Lepri, R. Livi, and A. Politi, *Phys. Rep.* **377**, 1 (2003).
- [40] B. Li, J. Wang, L. Wang, and G. Zhang, *Chaos* **15**, 015121 (2005).
- [41] A. Dhar, *Adv. Phys.* **57**, 457 (2008).
- [42] S. Nosé, *J. Chem. Phys.* **81**, 511 (1984).
- [43] W. G. Hoover, *Phys. Rev. A* **31**, 1695 (1985).
- [44] K. Xiong, M. Zhou, W. Liu, C. Zeng, and Z. Yan, *Chaos* **33**, 083144 (2023).
- [45] K. Xiong, J. Ren, F. Marchesoni, and J. Huang, *Phys. Rev. E* **108**, 044306 (2023).
- [46] C. Castellano and R. Pastor-Satorras, *Phys. Rev. Lett.* **105**, 218701 (2010).
- [47] C. W. Wu, *Nonlinearity* **18**, 1057 (2005).
- [48] J. J. Xiao, K. Yakubo, and K. W. Yu, *Phys. Rev. B* **73**, 054201 (2006).
- [49] G. Zhu, H. Yang, C. Yin, and B. Li, *Phys. Rev. E* **77**, 066113 (2008).
- [50] H. Wang, S. Hu, K. Takahashi, X. Zhang, H. Takamatsu, and J. Chen, *Nature Commun.* **8**, 15843 (2017).
- [51] L. Qiu, F. Li, N. Zhu, Y. Feng, X. Zhang, and X. Zhang, *Phys. Rev. B* **105**, 165406 (2022).
- [52] M. E. Itkis, F. Borondics, A. Yu, and R. C. Haddon, *Nano Lett.* **7**, 900 (2007).
- [53] R. S. Prasher, X. J. Hu, Y. Chalopin, N. Mingo, K. Lofgreen, S. Volz, F. Cleri, and P. Keblinski, *Phys. Rev. Lett.* **102**, 105901 (2009).
- [54] Y. Feng, X. Chen, Y. Li, Y. Wang, H. Li, and G. Zhou, *Macromol. Chem. Phys.* **222**, 2100200 (2021).
- [55] C. Huang, X. Qian, and R. Yang, *Mat. Sci. Eng. R* **132**, 1 (2018).